

# Multivariate Bicycle Codes

Lukas Voss,<sup>1, 2, 3, \*</sup> Sim Jian Xian,<sup>2, 4, †</sup> Tobias Haug,<sup>5, ‡</sup> and Kishor Bharti<sup>4, 6, 7, §</sup>

<sup>1</sup>*Institute of Theoretical Physics & IQST, Ulm University, Albert-Einstein-Allee 11, D-89069 Ulm, Germany*

<sup>2</sup>*Centre for Quantum Technologies, National University of Singapore, 3 Science Drive 2, Singapore 117543.*

<sup>3</sup>*Yale-NUS College, Singapore*

<sup>4</sup>*A\*STAR Quantum Innovation Centre (Q.InC), Institute of High Performance Computing (IHPC), Agency for Science, Technology and Research (A\*STAR), 1 Fusionopolis Way, #16-16 Connexis, Singapore, 138632, Republic of Singapore.*

<sup>5</sup>*Quantum Research Center, Technology Innovation Institute, Abu Dhabi, UAE*

<sup>6</sup>*Centre for Quantum Engineering, Research and Education, TCG CREST, Sector V, Salt Lake, Kolkata 700091, India.*

<sup>7</sup>*Science, Mathematics and Technology Cluster, Singapore University of Technology and Design, 8 Somapah Road, Singapore 487372, Singapore*

Quantum error correction suppresses noise in quantum systems to allow for high-precision computations. In this work, we introduce Multivariate Bicycle (MB) Quantum Low-Density Parity-Check (QLDPC) codes, via an extension of the framework developed by Bravyi *et al.* [Nature, 627, 778-782 (2024)] and particularly focus on Trivariate Bicycle (TB) codes. Unlike the weight-6 codes proposed in their study, we offer concrete examples of weight-4 and weight-5 TB-QLDPC codes which promise to be more amenable to near-term experimental setups. We show that our TB-QLDPC codes up to weight-6 have a bi-planar structure. Further, most of our new codes can also be arranged in a two-dimensional toric layout, and have substantially better encoding rates than comparable surface codes while offering similar error suppression capabilities. For example, we can encode 4 logical qubits with distance 5 into 30 physical qubits with weight-5 check measurements, while a surface code with these parameters requires 100 physical qubits. The high encoding rate and compact layout make our codes highly suitable candidates for near-term hardware implementations, paving the way for a realizable quantum error correction protocol.

*Introduction.*— Quantum computing promises to solve problems intractable for classical computers [1–3]. Despite advancements in improving hardware quality, noise remains the most significant challenge for realizing practical implementations to ultimately achieve both reliable and scalable quantum computations. As a consequence, quantum error correction (QEC) is required to reduce noise of the physical hardware [4, 5]. Among many QEC codes [6–8], the surface code has emerged which currently leads the forefront in experimental quantum computing due to its relatively high threshold error rates [8–13] and suitability for implementation with current hardware devices [14]. Despite its advantages, the surface code requires high qubit overhead leading to an asymptotically zero encoding rate while the distance scales as the square-root of the number of physical qubits [15].

Recently, Quantum Low-Density Parity-Check (QLDPC) codes have attracted attention for their potential to require less physical qubits than surface codes [16]. LDPC codes are well-established in classical error correction [17–19] for their efficiency and decoding performance. In a recent breakthrough [20], Bravyi *et al.* presented a set of QLDPC codes that are significantly more qubit-efficient than the surface code of the same number of logical qubits. These codes, called Bivariate Bicycle (BB) QLDPC codes, have origins in the work by Kovalev and Pryadko [21]. Ref. [20] introduced codes with weight-6 stabilizer checks which can be encoded into a bi-planar toric layout. This layout allows their code to accommodate four local stabilizer checks and two long-range checks. Still, finding codes

that reduce the weight of the stabilizer checks while maintaining good code properties could significantly simplify hardware implementations of QLPDC codes. Here, we introduce Multivariate Bicycle (MB) QLDPC codes to provide several novel low-weight codes with better encoding rates than comparable surface codes. We define MB-QLDPC codes in a general manner, and then focus on the concrete case of Trivariate Bicycle (TB) codes, which have three variable in the generating polynomials. For improved readability, we will from now on only use the term *code* to refer to a QLDPC code, if not explicitly stated otherwise. As a highlight, we find a weight-5 code with a single long-range check which encodes 4 logical qubits into only 30 physical qubits in a bi-planar toric architecture, while a comparable surface code would require 100 qubits. We analyze the performance of our codes under depolarizing noise, where we find comparable noise suppression to similar surface codes. We make progress on the properties of TB codes and prove that our codes up to weight-6 possess a bi-planar structure in Proposition 6 of SM F. This is not obvious given the choice of terms in the parity check matrices. Furthermore, we provide a weight-independent criterion to check whether a TB code has a toric layout structure in Proposition 2. We also show that all stabilizer checks are translational-invariant when the MB-QLDPC codes has a toric layout, further details to be found in Proposition 9. Finally, we show that weight-4 TB codes can possess a tangled toric layout, where the Tanner graph corresponds to a deformed torus with some mismatched edges.

*Framework.*— The group algebra of the multivariate bicycle code with  $r$  variables is  $G_r = \mathbb{Z}/l_1 \times \mathbb{Z}/l_2 \times \cdots \times \mathbb{Z}/l_r$ . In the special case of  $r = 2$ , we recover the group algebra of the BB code. The group  $G_r$  is isomor-

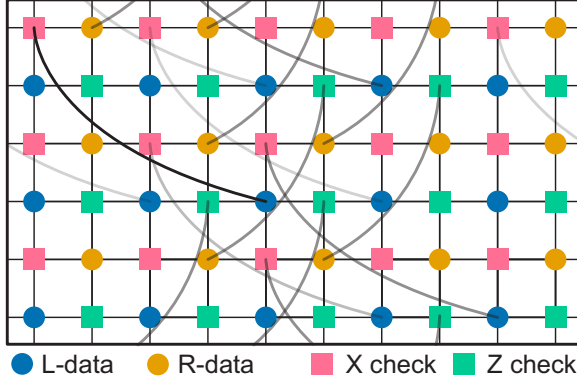


FIG. 1. Our weight-5  $[[30, 4, 5]]$  TB-QLDPC code can be arranged in a bi-planar grid with periodic boundary conditions (PBC) using 30 data qubits (which belong either to the L or R sublattice) and 30 qubits for parity check measurements. Each parity check involves four neighbouring data qubits, and one non-local interaction described by a translational invariant lattice vector  $(x, y)$ . For X-checks, the interaction vector is  $(-4, -3)$ , while for Z-checks we have  $(2, 3)$ . For better visibility, we only plot representatives of the non-local interactions at the center of the grid.

phic to the quotient of the multivariate polynomial ring  $R_r = \mathbb{F}_2[x_1, x_2, \dots, x_r]/(x_1^{l_1}-1, x_2^{l_2}-1, \dots, x_r^{l_r}-1)$ . Here, the quotient ring  $R_r$  has a basis consisting of the monomials  $x_1^{i_1} x_2^{i_2} \cdots x_r^{i_r}$ , where  $0 \leq i_1 \leq l_1-1, 0 \leq i_2 \leq l_2-1, \dots, 0 \leq i_r \leq l_r-1$ . In this work, we define the variable  $x_i$  using the following encoding:

1. Let  $enc(i) = b_q b_{q-1} \cdots b_2 b_1$  be the binary encoding of  $i$  using  $q = \lfloor \log r \rfloor + 1$  bits.
2. Let  $t_\alpha \equiv S_{l_i}^{b_\alpha}$  where  $S_{l_i}$  is a cyclic shift matrix of size  $l_i \times l_i$ .
3.  $x_i \equiv t_q \otimes t_{q-1} \otimes \cdots \otimes t_2 \otimes t_1$ .

Note that the above encoding is not unique and has been chosen for its simplicity and one can trivially define other encodings. Moreover, the different variables are not independent. For example, in the trivariate case, the quotient ring is given by

$$R_3 = \mathbb{F}_2[x_1, x_2, x_3]/(x_1^{l_1}-1, x_2^{l_2}-1, x_3-x_1 x_2).$$

In general, one can define variables such that they are all independent. For concreteness, in this work, we will focus on  $m = 3$  which will make them TB-QLDPC codes, a generalisation of BB-QLDPC codes discussed in Ref. [20, 22]. We start with the identity matrix  $I_m$  and the cyclic shift matrix  $S_l$  of size  $l \times l$  with  $(S_l)_{ij} = \delta_{j, (i+1) \bmod l}$  for integer-valued  $l$  and  $m$ . Previous BB codes are limited by

two only variables, namely  $x$  and  $y$ . Here, we introduce TB codes which are characterised by adding the third variable  $z$  of the form  $S_l \otimes S_m$ . Let now

$$x \equiv x_1 = S_l \otimes I_m, \quad y \equiv x_2 = I_l \otimes S_m, \quad z \equiv x_3 = S_l \otimes S_m$$

be matrices of dimension  $(l \cdot m) \times (l \cdot m)$  that commute with each other  $[x_i, x_j] = 0 \ \forall i, j \in \{1, 2, 3\}$ . Now, we define the pair of matrices

$$A = \sum_{j=1}^{\mathcal{W}_A} A_j \quad \text{and} \quad B = \sum_{j=1}^{\mathcal{W}_B} B_j \quad (1)$$

generating a code of weight  $\mathcal{W} = \mathcal{W}_A + \mathcal{W}_B$  with each matrix  $A_j$  and  $B_j$  being powers of  $x, y$  or  $z$ . Working in the binary field  $\mathbb{F}_2 = \{0, 1\}$ , we ensure avoiding cancellation of terms by only allowing for unique terms in both  $A$  and  $B$ . In order to fully describe a TB code, we need to further define the stabilizer check matrices

$$H_X = [A|B] \quad \text{and} \quad H_Z = [B^T|A^T]$$

Following this definition, we can then define  $X$ -type and  $Z$ -type check operators being a row  $v \in \mathbb{F}_2$  of  $H_X$  and  $H_Z$ , respectively. Since  $[A, B] = 0$ , these satisfy the stabilizer code condition requiring all  $X$ -type checks to commute with all  $Z$ -type checks, translating to  $H_X H_Z^T = 0$ . We emphasize that the  $A_j$  and  $B_j$  terms can be understood as introducing edges between checks and vertices on the Tanner Graph of the TB code, one per term. This viewpoint is crucial in understanding physical implementations in the Code Layout section. Further details can be found in SM F.

We then find the TB code with parameters  $[[n, k, d]]$  in accordance with Lemma 1 of Ref. [20]

$$\begin{aligned} n &= 2lm, & k &= 2 \cdot \dim(\ker(A) \cap \ker(B)) \\ d &= \min\{|v| : v \in \ker(H_X) \setminus \text{rs}(H_Z)\} \end{aligned} \quad (2)$$

with  $|v|$  as the Hamming weight of vector  $v$ .

*Results.*— In Table I, we provide an overview of our TB codes of weights four to seven. For a given distance  $d$  and number of logical qubits  $k$ , our codes require less physical qubits than surface codes which need  $n = kd^2$  physical qubits [8, 9]. Note that to encode  $k$  logical qubits via surface codes, one uses  $k$  rotated planar surface codes with  $d^2$  qubits each [20]. In Fig. 2, we illustrate decoding results under depolarizing noise for codes of stabilizer weights four and five. We performed decoding for physical error rates  $p$  down to  $10^{-3}$  and then extrapolate for lower error rates following a fit with Eq. (4).

In Table II in the SM, we present an overview of additional TB codes that outperform the surface code characteristics and provide a summary for the properties for codes of weights four to seven. We prove in Proposition 6 that our codes of weight-4 and weight-5 allow for a bi-

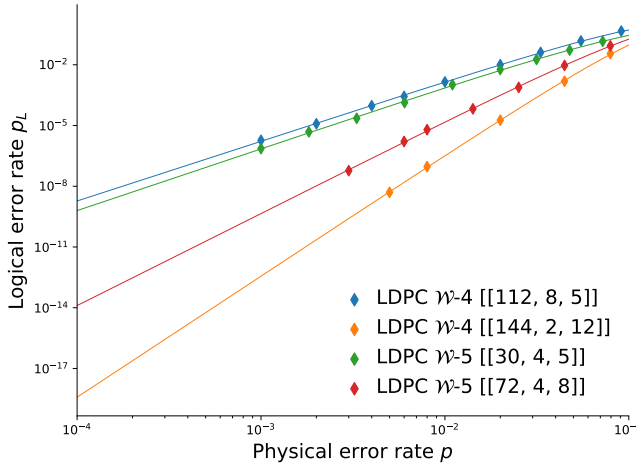


FIG. 2. Comparison of noise properties among our TB codes of weight-4 and weight-5. We find the fitted code distances  $d_{\text{fit}} = \{5.9, 12.0, 6.1, 8.3\}$ , respectively.

planar encoding architecture. This makes them suitable candidates for near-term hardware implementations.

For benchmarking, we compare our codes against planar surface codes with similar distance  $d$  and number of logical qubits  $k$ . In particular, the planar surface code of distance  $d$  can encode one logical qubit into a  $d \times d$  grid of physical qubits, leading to code parameters  $\llbracket d^2, 1, d \rrbracket$  [14]. To encode  $k$  logical qubits, we implement  $k$  instances of the planar surface code, resulting in a  $\llbracket kd^2, k, d \rrbracket$  code. The logical error probability per syndrome cycle  $p_L$  for  $k$  logical qubits can be directly computed from the logical error of a single planar surface code  $p_L(1)$  via [20]

$$p_L(k) = 1 - (1 - p_L(1))^k \quad (3)$$

with  $p_L(k)$  as the logical error probability of the surface code encoding  $k$  logical qubits. To characterize the error capabilities of our codes, we study the pseudo threshold  $p_0$ . It is defined as the value satisfying the break-even relation  $p_L(p) = k_p$  with  $k_p$  being the estimated probability that at least one unencoded qubit suffers an error. We fit the logical error  $p_L$  with the heuristic formula [20, 23]

$$p_L = p^{d_{\text{fit}}/2} \exp(c_0 + c_1 p + c_2 p^2) \quad (4)$$

where for surface codes and bicycle codes it has been observed that the fitted distance corresponds to the actual distance via  $d_{\text{fit}}/2 = \lceil d/2 \rceil$  [23].

In Fig. 3, we compare the noise suppression characteristics of our weight-5  $\llbracket 30, 4, 5 \rrbracket$  TB code (Fig. 1) with the weight-6  $\llbracket 72, 12, 6 \rrbracket$  code of Ref. [20] and the weight-6  $\llbracket 72, 8, 6 \rrbracket$  code of Ref. [24]. As a code of distance  $d$  can correct up to  $\lfloor (d-1)/2 \rfloor$  errors, all three codes can correct at most 2 errors. Also, all of them encoded into a bi-planar two-dimensional grid with toric layout. We note that to encode 8 logical qubits, one can take two independent

copies of our  $\llbracket 30, 4, 5 \rrbracket$  TB code to get a weight-5  $\llbracket 60, 8, 5 \rrbracket$  code. We highlight that this way, our TB code has a better encoding rate than the weight-6 BB code  $\llbracket 72, 8, 6 \rrbracket$  of Ref. [24]. Further, our code has only weight-5 parity checks and requires only one long-range connection, compared to the weight-6 checks with two long-range connections required by the codes of Refs. [20, 24].

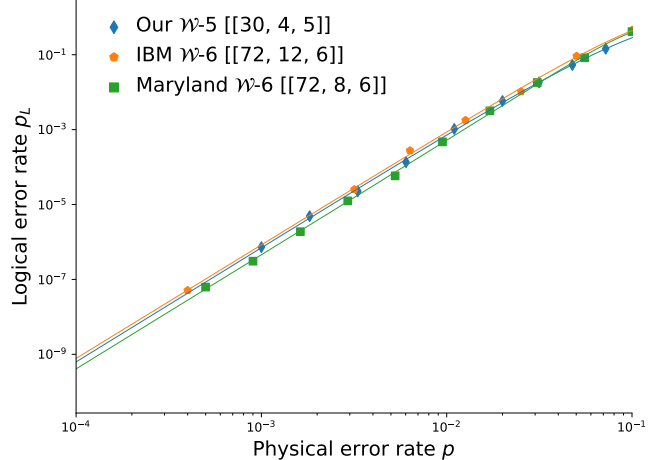


FIG. 3. Logical error rate of our weight-5  $\llbracket 30, 4, 5 \rrbracket$  TB code, weight-6  $\llbracket 72, 8, 6 \rrbracket$  BB code of Ref. [24], and weight-6  $\llbracket 72, 12, 6 \rrbracket$  BB code of Ref. [20].

*Code Layout.*— Here, we discuss the physical layout of qubits needed to implement our TB-QLDPC codes. We study two independent requirements, bi-planarity and a toric layout.

**Proposition 1** (Bi-planar Architecture). *All TB-QLDPC codes of weight-4, where  $A = A_1 + A_3$ ,  $B = B_1 + B_3$ , all codes of weight-5 such that  $A = A_1 + A_3$ ,  $B = B_1 + B_2 + B_3$ , and all codes of weight-6 such that  $A = A_1 + A_2 + A_3$ ,  $B = B_1 + B_2 + B_3$  (the case presented in Ref. [20]), or  $A = A_1 + A_3$ ,  $B = B_1 + B_2 + B_3 + B_4$  allow for a bi-planar architecture of thickness  $\theta = 2$ . The bi-planar decomposition can be computed in time  $O(n)$ .*

The proof is found in Proposition 6. It is currently unknown whether the weight-7 code is bi-planar.

Beyond bi-planarity, we use the concept of a toric layout to simplify the design process in physical implementations as elaborated in Proposition 5. We view the Tanner Graph as embedded on a torus, allowing for edge crossings, see Fig. 1.

**Definition 1** (Toric Layout [20]). *A TB-QLDPC code has a toric layout  $\iff \exists$  positive integers  $\mu, \lambda$  such that its Tanner Graph has a spanning sub-graph isomorphic to the Cayley Graph of  $\mathbb{Z}_{2\mu} \times \mathbb{Z}_{2\lambda}$ . The parameters  $2\mu$  and  $2\lambda$  determine the width and length of the toric layout for the MB code's Tanner Graph.*

Using the proposition below, we obtain an easy check for whether a TB code has a toric layout.

$\llbracket n, k, d \rrbracket$	$\mathcal{W}$	$r = k/n$	$r_{\text{TB}}/r_{\text{SC}}$	$p_0$	$p_{\text{L}}(10^{-4})$	toric	bi-planar
$\llbracket 144, 2, 12 \rrbracket$	4	1/72	2.0	0.1017	$4 \times 10^{-19}$	✗	✓
$\llbracket 30, 4, 5 \rrbracket$	5	1/7	3.3	0.0437	$6 \times 10^{-10}$	✓	✓
$\llbracket 30, 6, 4 \rrbracket$	6	1/5	3.2	0.0234	$3 \times 10^{-7}$	✓	✓
$\llbracket 30, 4, 5 \rrbracket$	7	1/7	3.3	0.0507	$5 \times 10^{-10}$	✓	unknown

TABLE I. Selection of TB-QLDPC codes ordered by weight  $\mathcal{W}$  of the stabilizer checks. The code parameters  $\llbracket n, k, d \rrbracket$  correspond to  $k$  logical qubits,  $n$  physical qubits and code distance  $d$ . The encoding rate  $r = k/n$  is rounded to the next smallest integer value. In column  $r_{\text{TB}}/r_{\text{SC}}$ , we show the improvement factor in encoding rate compared to a surface code with the same code distance and number of logical qubits. The last two columns provide the pseudo-threshold  $p_0$  and the logical error  $p_{\text{L}}$  at the physical error rate at  $p = 10^{-4}$  which we gain from a fit with Eq. (4). We use a depolarizing error model without readout error.

**Proposition 2** (TB-QLDPC Toric Layout Criterion for arbitrary weight, generalised from Ref. [20]). *A TB-QLDPC code ( $QC(A, B)$ ) of weight  $\mathcal{W} = \mathcal{W}_A + \mathcal{W}_B$  has a toric layout  $\iff \exists i, j \in \{1, \dots, \mathcal{W}_A\}, g, h \in \{1, \dots, \mathcal{W}_B\}$  such that*

1.  $\langle A_i A_j^T, B_g B_h^T \rangle = M$  and
2.  $\text{ord}(A_i A_j^T) \text{ord}(B_g B_h^T) = lm$ .

We discuss further intuition in Ref. 8.

Although Ref. [20] proves Proposition 2 for the weight-6 case where  $A = A_1 + A_2 + A_3$ ,  $B = B_1 + B_2 + B_3$ , we emphasize that the proposition holds more generally because none of their argument requires that  $i, j, g, h \in \{1, 2, 3\}$ . In fact, we may carry out an identical argument for generic weights  $A = \sum_{j=1}^{\mathcal{W}_A} A_j$  and  $B = \sum_{j=1}^{\mathcal{W}_B} B_j$ . As an example of the generality of Proposition 2, our weight-7  $\llbracket 30, 4, 5 \rrbracket$  code was numerically confirmed to have a toric layout, see Table II.

Note that since  $r = 2$  for our code, our toric layout criterion and results are on 2-dimensional Euclidean space which is experimentally relevant. If our multivariate group algebra was comprised was  $r$  independent variables, we obtain an analogous toric layout definition and criterion on an  $r$ -dimensional torus for  $\mathbb{Z}_{2\mu_1} \times \dots \times \mathbb{Z}_{2\mu_r}$ , which experiment is not ready to realize. This higher dimensional toric layout arises because each independent variable introduces an independent orthogonal direction in Euclidean space.

**Proposition 3** (TB-QLDPC Toric Layout Edge Translational Invariance). *For any TB-QLDPC code (with Tanner Graph  $G$ ) of sparsity  $\mathcal{W}$  with a toric layout, for any vertex  $v_T$  of a fixed type  $T \in \{L, R, X, Z\}$ , all of the  $\mathcal{W}$  edges of  $v_T$ , including the long-range edges, have translationally invariant interaction vectors on the toric layout.*

For a weight- $\mathcal{W}$  TB code, four interactions remain local, while  $\mathcal{W} - 4$  interactions are non-local with translational symmetry. An example is shown in Fig. 1. The key property allowing this is the cyclic property of  $H_X$  and  $H_Z$  for such codes, elaborated in the Supplemental

Material (SM) [25]. An analogous proposition holds for MB codes with a toric layout as well, by repeating the arguments in higher spatial dimensions.

Using the test in Proposition 2, we further conclude that all the weight-4 codes do not have a toric layout. However, they can possess a tangled toric layout (see Def 9), such as in Fig 4 by using the tool from Ref. [26].

Intuitively, a tangled toric layout means that the code behaves as a surface code in the bulk, but with long-range edges produced by modifying the PBC along the horizontal and vertical edges of the square grid. This minor modification makes it potentially more attractive than bi-planar architectures when taking a first step beyond the toric code. In the Bravyi-Poulin-Terhal (BPT) bound  $kd^2 \leq cn$  [27], for the toric code the locality constant  $c = 1$  saturates the bound, but in our weight-4  $\llbracket 64, 2, 8 \rrbracket$  code we would need  $c = 2$ , verifying its enhanced performance. We provide an  $O(n)$  algorithm to determine the tangling parameters  $(\sigma, \tau)$ . This algorithm applies more generally to two-block codes, defined as CSS QLDPC codes such that  $H_X = [A|B]$  and  $H_Z = [B^T|A^T]$ , where A and B commute and have the same size.

**Proposition 4** (Algorithm for Weight-4  $(\sigma, \tau)$ -Tangled Toric Layout Parameters). *For any two-block CSS QLDPC code of sparsity 4 with equal X and Z degree per data qubit (2 each), suppose it has a tangled toric layout known to have torus parameters  $\mu, \lambda$ . Then there is an  $O(n)$  time algorithm to find  $\sigma, \tau$ .*

The key idea of the algorithm is to embed a spanning subgraph onto the rectangular 2-D grid of size  $2\mu \times 2\lambda$ . The unassigned edges on the grid give us  $\sigma$  and  $\tau$  respectively. Details in Proposition 10.

*Discussion.*— In this work, we introduce MB-QLDPC codes as multi-variable generalisation of BB-QLDPC codes, which have only two variables. We study TB-QLDPC with three variables in detail and present compact codes with high encoding rates and strong noise suppression. Moreover, by optimised search we find codes with more resource-efficient parameters than corresponding surface codes. We obtain promising codes with only weights four and five, which could offer a more

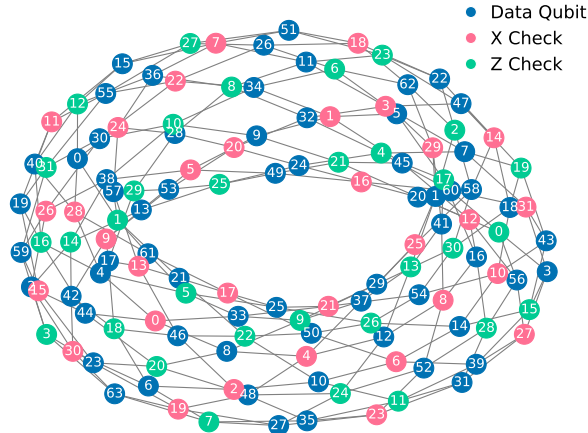


FIG. 4. Tanner Graph of the weight-4  $[[64, 2, 8]]$  code, as a tangled torus with layout parameters  $\mu = l = 8, \lambda = m = 4$ . The usual torus topology is disrupted by a tangle on the right side of the figure.

hardware-friendly implementation compared to recently found weight six BB-QLDPC codes from Ref. [20, 24, 28]. For example, we find a highly compact weight-5  $[[30, 4, 5]]$  code which has a toric bi-planar layout and a single long-range connection, which shows promise for practical implementations on current hardware. Further, we make progress on the properties of TB-QLDPC codes: We show that up to weight-6, all TB-QLDPC codes have conveniently a bi-planar structure. Additionally, we provide methods to check whether TB-QLDPC codes have a toric layout, which could be used to systematically search for codes with experimental-friendly layout, significantly reducing the search space of codes. Future research directions are discussed in SM E.

*Acknowledgments.*— We thank Sergey Bravyi and Patrick Rall for a fruitful discussion in the beginning of the project. LV acknowledges the financial support by the Baden-Württemberg Foundation and the Ernst-Wilken Foundation for his research stay at CQT. This research is supported by A\*STAR C230917003.

- [4] D. J. MacKay and R. M. Neal, Near Shannon limit performance of low density parity check codes, *Electronics letters* **33**, 457 (1997).
- [5] S. Resch and U. R. Karpuzcu, Benchmarking quantum computers and the impact of quantum noise, *ACM Computing Surveys (CSUR)* **54**, 1 (2021).
- [6] P. W. Shor, Scheme for reducing decoherence in quantum computer memory, *Physical review A* **52**, R2493 (1995).
- [7] A. Steane, Multiple-particle interference and quantum error correction, *Proceedings of the Royal Society of London. Series A: Mathematical, Physical and Engineering Sciences* **452**, 2551 (1996).
- [8] A. Y. Kitaev, Fault-tolerant quantum computation by anyons, *Annals of physics* **303**, 2 (2003).
- [9] S. B. Bravyi and A. Y. Kitaev, Quantum codes on a lattice with boundary, *arXiv preprint quant-ph/9811052* (1998).
- [10] A. G. Fowler, A. M. Stephens, and P. Groszkowski, High-threshold universal quantum computation on the surface code, *Physical Review A* **80**, 052312 (2009).
- [11] A. G. Fowler, A. C. Whiteside, and L. C. Hollenberg, Towards practical classical processing for the surface code, *Physical review letters* **108**, 180501 (2012).
- [12] Y. Zhao, Y. Ye, H.-L. Huang, Y. Zhang, D. Wu, H. Guan, Q. Zhu, Z. Wei, T. He, S. Cao, *et al.*, Realization of an error-correcting surface code with superconducting qubits, *Physical Review Letters* **129**, 030501 (2022).
- [13] A. Asfaw, A. Megrant, C. Jones, C. Gidney, D. Bacon, D. Debroy, D. Kafri, E. Lucero, H. Neven, J. Hilton, *et al.*, Suppressing quantum errors by scaling a surface code logical qubit, *Nature* **614**, 676 (2023).
- [14] Suppressing quantum errors by scaling a surface code logical qubit, *Nature* **614**, 676 (2023).
- [15] D. Gottesman, An introduction to quantum error correction and fault-tolerant quantum computation, in *Quantum information science and its contributions to mathematics, Proceedings of Symposia in Applied Mathematics*, Vol. 68 (2010) pp. 13–58.
- [16] N. P. Breuckmann and J. N. Eberhardt, Quantum low-density parity-check codes, *PRX Quantum* **2**, 040101 (2021).
- [17] D. J. MacKay, *Information theory, inference and learning algorithms* (Cambridge university press, 2003).
- [18] A. Shokrollahi, LDPC codes: An introduction, in *Coding, cryptography and combinatorics* (Springer, 2004) pp. 85–110.
- [19] T. K. Moon, *Error correction coding: mathematical methods and algorithms* (John Wiley & Sons, 2020).
- [20] S. Bravyi, A. W. Cross, J. M. Gambetta, D. Maslov, P. Rall, and T. J. Yoder, High-threshold and low-overhead fault-tolerant quantum memory, *Nature* **627**, 778 (2024).
- [21] A. A. Kovalev and L. P. Pryadko, Quantum kronecker sum-product low-density parity-check codes with finite rate, *Physical Review A* **88**, 012311 (2013).
- [22] D. J. MacKay, G. Mitchison, and P. L. McFadden, Sparse-graph codes for quantum error correction, *IEEE Transactions on Information Theory* **50**, 2315 (2004).
- [23] S. Bravyi and A. Vargo, Simulation of rare events in quantum error correction, *Physical Review A* **88**, 062308 (2013).
- [24] N. Berthelsen, D. Devulapalli, E. Schoute, A. M. Childs, M. J. Gullans, A. V. Gorshkov, and D. Gottesman, Toward a 2D local implementation of quantum LDPC

\* [lukas\\_voss@icloud.com](mailto:lukas_voss@icloud.com)

† [simjianxian@u.nus.edu](mailto:simjianxian@u.nus.edu)

‡ [tobias.haug@u.nus.edu](mailto:tobias.haug@u.nus.edu)

§ [kishor.bharti1@gmail.com](mailto:kishor.bharti1@gmail.com)

- [1] P. W. Shor, Polynomial-time algorithms for prime factorization and discrete logarithms on a quantum computer, *SIAM review* **41**, 303 (1999).
- [2] S. Arora and B. Barak, *Computational complexity: a modern approach* (Cambridge University Press, 2009).
- [3] M. A. Nielsen and I. L. Chuang, *Quantum computation and quantum information*, Vol. 2 (Cambridge university press Cambridge, 2001).

codes, arXiv preprint arXiv:2404.17676 (2024).

[25] See Supplemental Material for detailed derivations, as well as additional theoretical and numerical results.

[26] A. Hagberg, P. Swart, and D. S Chult, *Exploring network structure, dynamics, and function using NetworkX*, Tech. Rep. (Los Alamos National Lab.(LANL), Los Alamos, NM (United States), 2008).

[27] S. Bravyi, D. Poulin, and B. Terhal, Tradeoffs for reliable quantum information storage in 2d systems, *Physical Review Letters* **104**, 10.1103/physrevlett.104.050503 (2010).

[28] T. R. Scruby, T. Hillmann, and J. Roffe, High-threshold, low-overhead and single-shot decodable fault-tolerant quantum memory, arXiv:2406.14445 (2024).

[29] D. Gottesman, *Stabilizer codes and quantum error correction* (California Institute of Technology, 1997).

[30] A. R. Calderbank, E. M. Rains, P. W. Shor, and N. J. Sloane, Quantum error correction and orthogonal geometry, *Physical Review Letters* **78**, 405 (1997).

[31] A. R. Calderbank and P. W. Shor, Good quantum error-correcting codes exist, *Physical Review A* **54**, 1098 (1996).

[32] J.-P. Tillich and G. Zémor, Quantum LDPC codes with positive rate and minimum distance proportional to the square root of the blocklength, *IEEE Transactions on Information Theory* **60**, 1193 (2013).

[33] M. B. Hastings, J. Haah, and R. O'Donnell, Fiber bundle codes: breaking the  $n^{1/2} \text{polylog}(n)$  barrier for quantum ldpc codes, in *Proceedings of the 53rd Annual ACM SIGACT Symposium on Theory of Computing* (2021) pp. 1276–1288.

[34] P. Panteleev and G. Kalachev, Quantum LDPC codes with almost linear minimum distance, *IEEE Transactions on Information Theory* **68**, 213 (2021).

[35] P. Panteleev and G. Kalachev, Asymptotically good quantum and locally testable classical LDPC codes, in *Proceedings of the 54th Annual ACM SIGACT Symposium on Theory of Computing* (2022) pp. 375–388.

[36] A. Leverrier and G. Zémor, Quantum tanner codes, in *2022 IEEE 63rd Annual Symposium on Foundations of Computer Science (FOCS)* (IEEE, 2022) pp. 872–883.

[37] I. Dinur, M.-H. Hsieh, T.-C. Lin, and T. Vidick, Good quantum LDPC codes with linear time decoders, in *Proceedings of the 55th annual ACM symposium on theory of computing* (2023) pp. 905–918.

[38] S. Bravyi, M. Suchara, and A. Vargo, Efficient algorithms for maximum likelihood decoding in the surface code, *Physical Review A* **90**, 032326 (2014).

[39] A. J. Ferris and D. Poulin, Tensor networks and quantum error correction, *Physical review letters* **113**, 030501 (2014).

[40] E. Dennis, A. Kitaev, A. Landahl, and J. Preskill, Topological quantum memory, *Journal of Mathematical Physics* **43**, 4452 (2002).

[41] G. Torlai and R. G. Melko, Neural decoder for topological codes, *Physical review letters* **119**, 030501 (2017).

[42] N. Delfosse and N. H. Nickerson, Almost-linear time decoding algorithm for topological codes, *Quantum* **5**, 595 (2021).

[43] O. Higgott and C. Gidney, Sparse blossom: correcting a million errors per core second with minimum-weight matching, arXiv:2303.15933 (2023).

[44] J. Roffe, D. R. White, S. Burton, and E. Campbell, Decoding across the quantum low-density parity-check code landscape, *Physical Review Research* **2**, 043423 (2020).

[45] P. Panteleev and G. Kalachev, Degenerate quantum ldpc codes with good finite length performance, *Quantum* **5**, 585 (2021).

[46] D. Poulin, Stabilizer formalism for operator quantum error correction, *Physical review letters* **95**, 230504 (2005).

[47] S. Bravyi, G. Duclos-Cianci, D. Poulin, and M. Suchara, Subsystem surface codes with three-qubit check operators, arXiv:1207.1443 (2012).

[48] M. B. Hastings and J. Haah, Dynamically generated logical qubits, *Quantum* **5**, 564 (2021).

[49] C. Gidney, M. Newman, A. Fowler, and M. Broughton, A fault-tolerant honeycomb memory, *Quantum* **5**, 605 (2021).

[50] C. Vuillot, Planar floquet codes, arXiv preprint arXiv:2110.05348 (2021).

[51] J. Haah and M. B. Hastings, Boundaries for the honeycomb code, *Quantum* **6**, 693 (2022).

[52] O. Higgott and N. P. Breuckmann, Constructions and performance of hyperbolic and semi-hyperbolic floquet codes, arXiv preprint arXiv:2308.03750 (2023).

[53] A. Fahimniya, H. Dehghani, K. Bharti, S. Mathew, A. J. Kollár, A. V. Gorshkov, and M. J. Gullans, Fault-tolerant hyperbolic floquet quantum error correcting codes, arXiv preprint arXiv:2309.10033 (2023).

[54] H. Bombin, D. Litinski, N. Nickerson, F. Pastawski, and S. Roberts, Unifying flavors of fault tolerance with the zx calculus, arXiv preprint arXiv:2303.08829 (2023).

[55] A. Townsend-Teague, J. M. de la Fuente, and M. Kesselring, Floquetifying the colour code, arXiv:2307.11136 (2023).

[56] A. Tanggara, M. Gu, and K. Bharti, Strategic code: A unified spatio-temporal framework for quantum error-correction, arXiv preprint arXiv:2405.17567 (2024).

[57] J. A. Bondy and U. S. R. Murty, *Graph Theory* (Springer London, 2008).

[58] H.-K. Lin and L. P. Pryadko, Quantum two-block group algebra codes (2023), arXiv:2306.16400.

[59] P. Mutzel, T. Odenthal, and M. Scharbrodt, The thickness of graphs: A survey, *Graphs and Combinatorics* **14**, 59–73 (1998).

[60] A. Mansfield, Determining the thickness of graphs is np-hard, *Mathematical Proceedings of the Cambridge Philosophical Society* **93**, 9–23 (1983).

[61] H. DE FRAYSSEIX, P. O. DE MENDEZ, and P. ROSENSTIEHL, Trémaux trees and planarity, *International Journal of Foundations of Computer Science* **17**, 1017–1029 (2006).

[62] R. Sarkar and T. J. Yoder, A graph-based formalism for surface codes and twists, arXiv:2101.09349 (2023).

## Supplemental Material

We provide proofs and additional details supporting the claims in the main text.

### Appendix A: Codes overview

#### Weight-4 QLDPC Codes

$[n, k, d]$	$r$	$l, m$	$r_{\text{BB}}/r_{\text{SC}}$	$p_0$	$p_L(10^{-4})$	$A$	$B$	$i, j, g, h$	$\mu, \lambda$	toric	bi-planar
$[112, 8, 5]$	$1/14$	$7, 8$	$1.8$	$0.0298$	$2 \times 10^{-9}$	$z^2 + z^6$	$x + x^6$	$\times$	$\times$	$\times$	$\checkmark$
$[64, 2, 8]$	$1/32$	$8, 4$	$2.0$	$0.0767$	$4 \times 10^{-13}$	$x + x^2$	$x^3 + y$	$\times$	$\times$	$\times$	$\checkmark$
$[72, 2, 8]$	$1/36$	$4, 9$	$1.8$	$0.0863$	$2 \times 10^{-13}$	$x + y^2$	$x^2 + y^2$	$\times$	$\times$	$\times$	$\checkmark$
$[96, 2, 8]$	$1/48$	$6, 8$	$1.3$	$0.0911$	$4 \times 10^{-16}$	$x^5 + y^6$	$z + z^4$	$\times$	$\times$	$\times$	$\checkmark$
$[112, 2, 10]$	$1/56$	$7, 8$	$1.8$	$0.097$	$2 \times 10^{-16}$	$z^6 + x^5$	$z^2 + y^5$	$\times$	$\times$	$\times$	$\checkmark$
$[144, 2, 12]$	$1/72$	$8, 9$	$2.0$	$0.1017$	$4 \times 10^{-19}$	$x^3 + y^7$	$x + y^5$	$\times$	$\times$	$\times$	$\checkmark$

#### Weight-5 QLDPC Codes

$[n, k, d]$	$r$	$l, m$	$r_{\text{BB}}/r_{\text{SC}}$	$p_0$	$p_L(10^{-4})$	$A$	$B$	$i, j, g, h$	$\mu, \lambda$	toric	bi-planar
$[30, 4, 5]$	$1/7$	$3, 5$	$3.3$	$0.0437$	$6 \times 10^{-10}$	$x + z^4$	$x + y^2 + z^2$	$(1, 2, 2, 3)$	$(5, 3)$	$\checkmark$	$\checkmark$
$[72, 4, 8]$	$1/18$	$4, 9$	$3.6$	$0.0785$	$8 \times 10^{-14}$	$x + y^3$	$x^2 + y + y^2$	$\times$	$\times$	$\times$	$\checkmark$
$[96, 4, 8]$	$1/24$	$8, 6$	$2.7$	$0.0823$	$1 \times 10^{-13}$	$x^6 + x^3$	$z^5 + x^5 + y$	$(1, 2, 1, 2)$	$(8, 6)$	$\checkmark$	$\checkmark$

#### Weight-6 QLDPC Codes

$[n, k, d]$	$r$	$l, m$	$r_{\text{BB}}/r_{\text{SC}}$	$p_0$	$p_L(10^{-4})$	$A$	$B$	$i, j, g, h$	$\mu, \lambda$	toric	bi-planar
$[30, 6, 4]$	$1/5$	$5, 3$	$3.2$	$0.0234$	$3 \times 10^{-7}$	$x^4 + z^3$	$x^4 + x + z^4 + y$	$(1, 2, 1, 3)$	$(5, 3)$	$\checkmark$	$\checkmark$
$[48, 6, 6]$	$1/8$	$4, 6$	$4.5$	$0.0495$	$2 \times 10^{-10}$	$x^2 + y^4$	$x^3 + z^3 + y^2 + y$	$\times$	$\times$	$\times$	$\checkmark$
$[40, 4, 6]$	$1/10$	$4, 5$	$3.6$	$0.0588$	$7 \times 10^{-11}$	$x^2 + y$	$y^4 + y^2 + x^3 + x$	$\times$	$\times$	$\times$	$\checkmark$
$[48, 4, 6]$	$1/12$	$4, 6$	$3.0$	$0.0698$	$3 \times 10^{-11}$	$x^3 + y^5$	$x + z^5 + y^5 + y^2$	$(1, 2, 3, 4)$	$(12, 2)$	$\checkmark$	$\checkmark$

#### Weight-7 QLDPC Codes

$[n, k, d]$	$r$	$l, m$	$r_{\text{BB}}/r_{\text{SC}}$	$p_0$	$p_L(10^{-4})$	$A$	$B$	$i, j, g, h$	$\mu, \lambda$	toric	bi-planar
$[30, 4, 5]$	$1/7$	$5, 3$	$3.3$	$0.0507$	$5 \times 10^{-10}$	$x^4 + x^2$	$x + x^2 + y + z^2 + z^3$	$(1, 2, 2, 4)$	$(5, 3)$	$\checkmark$	$\times$

TABLE II. Summary of QLDPC codes sorted by encoding rate  $r = k/n$ . For each code, we provide the improvement in qubit-efficiency  $r_{\text{BB}}/r_{\text{SC}}$  compared to the surface code, the physical error-rate below which error correction becomes a net-gain also known as the pseudo-threshold  $p_0$  and the respective code polynomials  $A$  and  $B$ .  $i, j, g, h$  refer to the indices chosen to satisfy a toric layout, with  $\mu, \lambda$  as the torus parameters such that the torus is embedded on a  $2\mu \times 2\lambda$  grid with periodic boundary conditions. If no suitable indices could be found that allow for a toric layout, the column value is set to  $\times$ .

## Appendix B: Selected Codes of different weight

*Weight-4.*— In Fig. 5, we show the physical error rate  $p$  against the logical error rate  $p_L$  for our weight-4 QLDPC code  $[[112, 8, 5]]$ . As comparison, we also show surface codes with the same number of logical qubits and similar distance  $d$ . We find that our code has comparable error suppression than the  $[[200, 8, 5]]$  surface code, while requiring only about half the number of physical qubits. We also fit the logical error rates with Eq. (4), where for our code we find a fitted code distance  $d_{\text{fit}} = 5.9$ .

*Weight-5.*— Next, in Fig. 6 we study the error suppression of our  $[[30, 4, 5]]$  code, which is a weight-5 TB code, who's layout is shown in Fig. 1. Our code suppresses logical errors at a physical error rate  $p = 10^{-3}$  by more than three orders of magnitude, allows for a toric bi-planar layout and has about three times higher encoding rate compared to the  $[[100, 4, 5]]$  surface code which has similar error suppression.

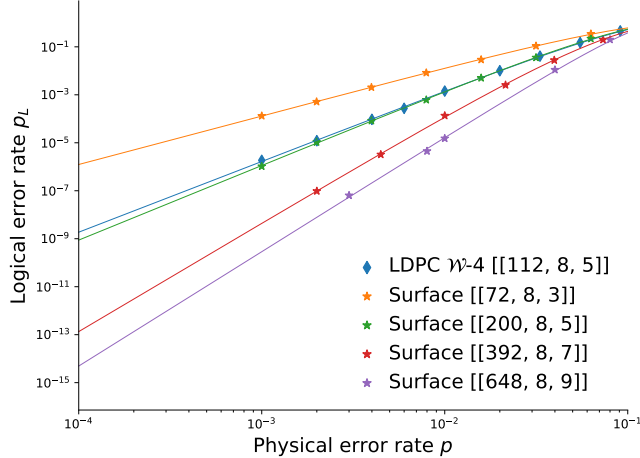


FIG. 5. Logical error rate  $p_L$  against physical error rate  $p$  for our weight-4 code  $[[112, 8, 5]]$ , and surface codes with similar code parameters. The error curves are fitted with Eq. (4), yielding a fitted code distance of  $d_{\text{fit}} = 5.9$ .

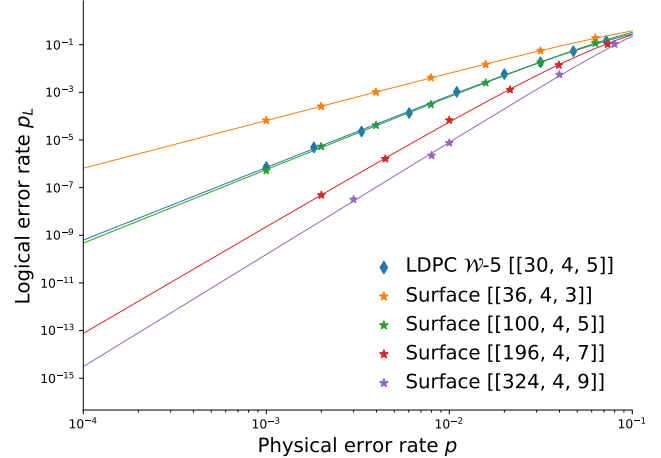


FIG. 6. Logical error rate  $p_L$  against physical error rate  $p$  for our weight-5 code  $[[30, 4, 5]]$ . We show surface codes with comparable code parameters as reference. We find  $d_{\text{fit}} = 6.1$  for our QLDPC code.

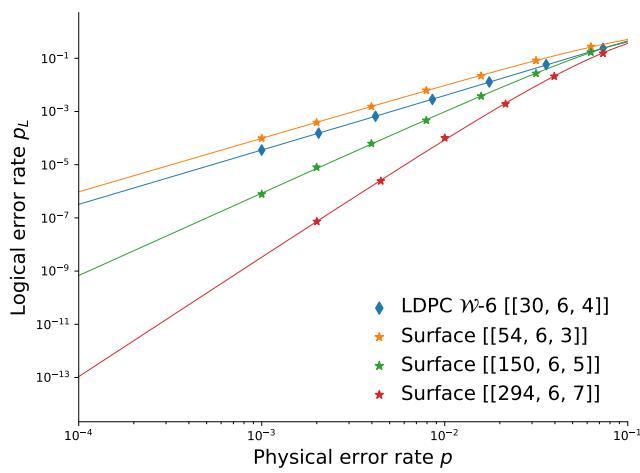


FIG. 7. Logical error rate of our weight-6 code  $[[30, 6, 4]]$  against comparable surface codes. We find  $d_{\text{fit}} = 4.1$ .

*Weight-6.*— In Fig. 7, we present our weight-6  $[[30, 6, 4]]$  code which has a high encoding rate of  $1/5$  and find it to have a toric layout with bi-planar structure. We find comparable error suppression scaling as the distance 3 surface code. At physical error rate  $p = 10^{-3}$ , we find a logical error rate of  $3.5 \times 10^{-5}$  corresponding to a logical noise

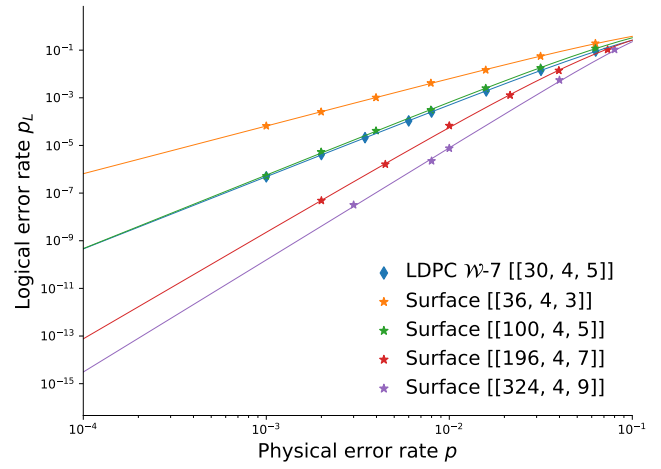


FIG. 8. Our weight-7 code  $[[30, 4, 5]]$  compared against surface codes with the same number of logical qubits. We find  $d_{\text{fit}} = 6.1$ .

suppression by two orders of magnitude. We note that a surface code with distance-4 and the same number of logical qubits requires 96 physical qubits, making our code three times more qubit efficient.

*Weight 7.*— Now, in Fig. 8, we study our weight-7 code with parameters  $[[30, 4, 5]]$ . Note that we also found a weight-5 code with the same code parameters. We find that our weight-7  $[[30, 4, 5]]$  code has similar error suppression than the  $[[100, 4, 5]]$  surface code.

### Appendix C: Decoding performance

We show noise suppression performance for our QLDPC codes of weight six under depolarizing noise. In Figs. 9 - 12, we show our codes in comparison with a selection of surface code of lower and higher distance than the QLDPC code to illustrate the noise performance. Since a surface code architecture would require  $k$  batches of a  $d \times d$  grid of qubits, the total number of physical qubits required to implement  $k$  logical qubits at code distance  $d$  reads  $n = kd^2$ .

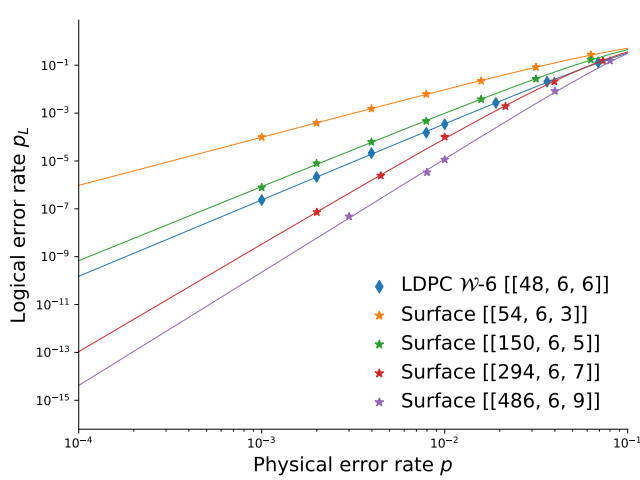


FIG. 9. Our weight-6 code  $[[48, 6, 6]]$  has a lower logical error rate than the distance-5 surface code while requiring three times less qubits coming with an encoding rate of  $1/8$ .

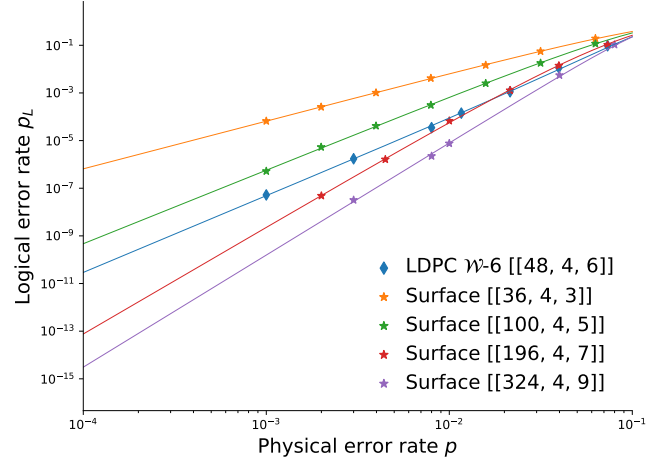


FIG. 10. Our weight-6 code  $[[48, 4, 6]]$  has an encoding rate of  $1/12$ . We only need a third of the number of physical qubits compared to the distance-6 surface code to correct up to 2 error before a logical one would occur.

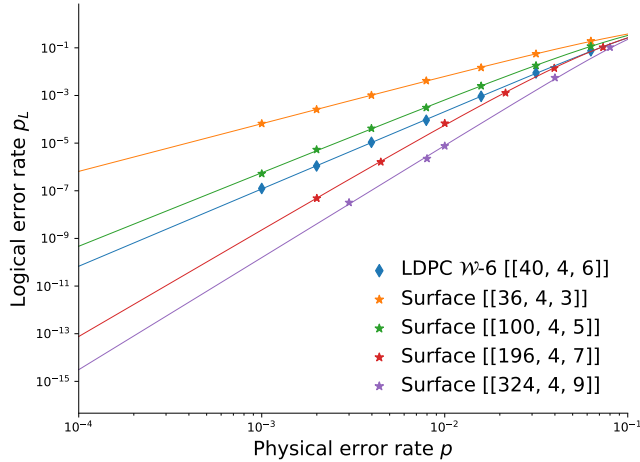


FIG. 11. We present a weight-6 with an encoding rate of 10% and parameters  $[[40, 4, 6]]$ . Compared to the distance-6 surface code, our code requires less physical qubits by a factor of 3.6.

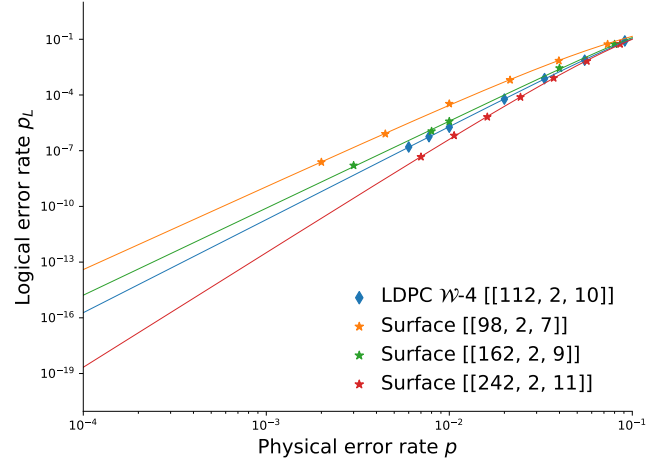


FIG. 12. This weight-4 code  $[[112, 2, 10]]$  requires about half the number of physical qubits compared to the surface code.

Next, we show the noise suppression performance for QLDPC codes of weight four under depolarizing noise. In Figs. 13 - 15, we show our codes in comparison with a selection of surface code of lower and higher distance than the QLDPC code to illustrate the noise performance. Since a surface code architecture would require  $k$  batches of a  $d \times d$  grid of qubits, the total number of physical qubits required to implement  $k$  logical qubits at code distance  $d$  reads  $n = kd^2$ .

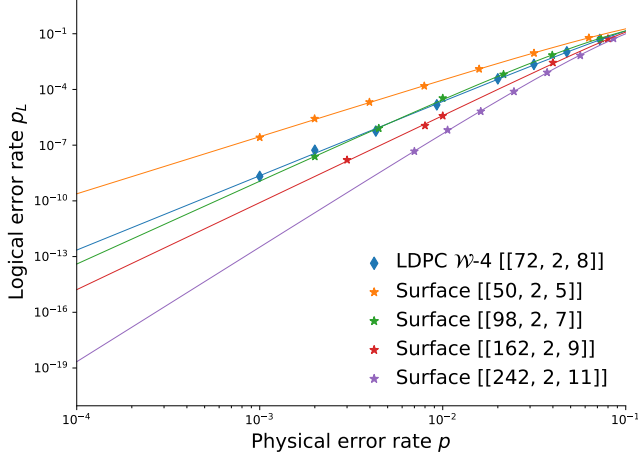


FIG. 13. Our weight-4 code  $[[72, 2, 8]]$  offers a high code distance while just using almost half of the number of physical qubits than the surface code would require.

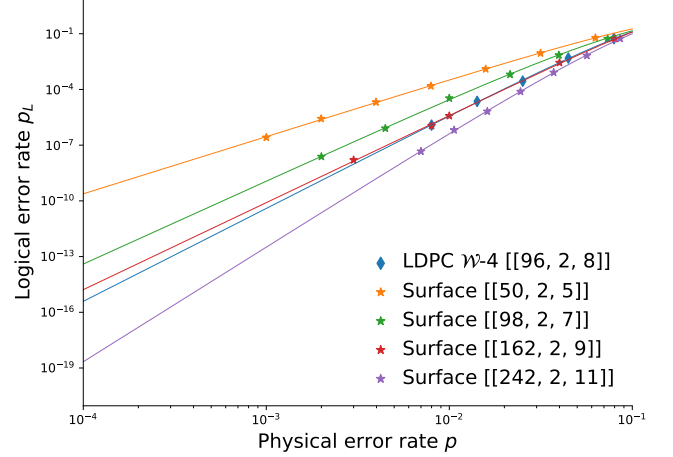


FIG. 14. Our weight-4 code  $[[96, 2, 8]]$  provides good noise suppression characteristics and requires less physical qubits than the equivalent surface by 33%.

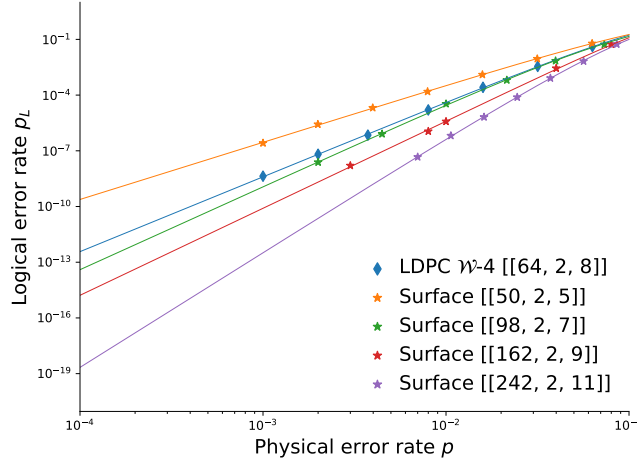


FIG. 15. Our weight-4 code  $[[64, 2, 8]]$  encodes two logical qubits at only half the resources needed for a surface code implementation.

Finally, we show the suppression performance for QLDPC codes of weight five under depolarizing noise. In Figs. 16 - 17, we show our code in comparison with a selection of surface code of lower and higher distance than the code to illustrate the noise performance. Since a surface code architecture would require  $k$  batches of a  $d \times d$  grid of qubits, the total number of physical qubits required to implement  $k$  logical qubits at code distance  $d$  reads  $n = kd^2$ .

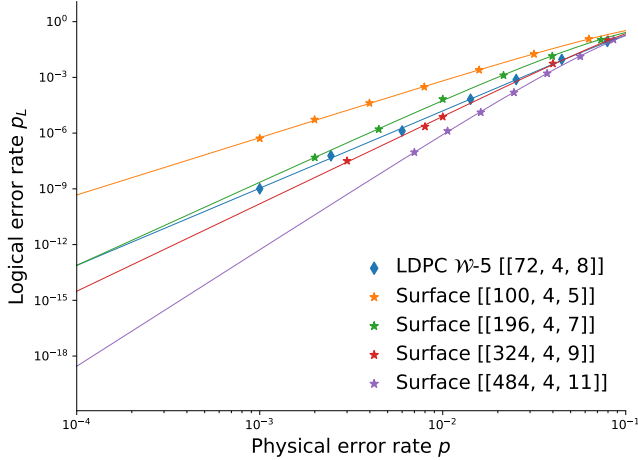


FIG. 16. Our weight-5 code  $[[72, 4, 8]]$  shows better noise performance than the distance-7 surface code and is more qubit efficient by a factor of 2.7. We find a fitted code distance of 8.3.

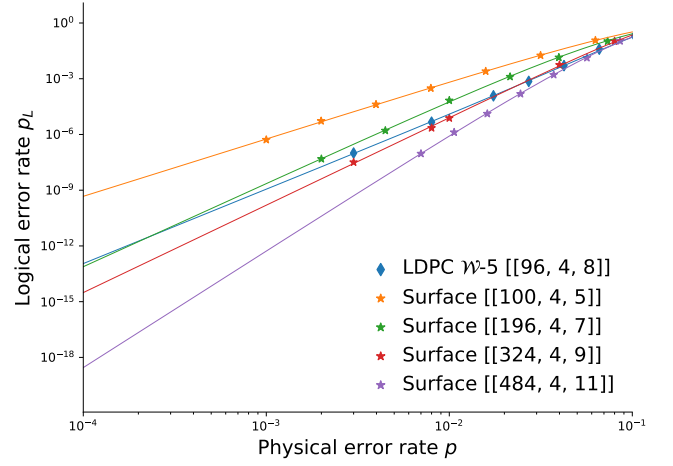


FIG. 17. With our weight-5 code  $[[96, 4, 8]]$  we provide a mix out of high code distance and moderate encoding rate. Further, an implementation requires less physical qubits than the distance-8 surface code by almost a factor of 2.7.

## Appendix D: Background

QEC codes are essential for executing high-fidelity computations on noisy quantum computers. Without QEC, errors accumulate during circuit execution, yielding an unreliable output. Stabilizer codes [29, 30] represent a class of QEC codes defined by their stabilizer group, which is an abelian subgroup of the Pauli group on  $n$  qubits that keeps the codespace invariant. The codespace of a stabilizer code is equivalently described as the joint  $+1$ -eigenspace of the stabilizer generators  $S = \langle S_1, S_2, \dots, S_r \rangle$ . For a  $[[n, k, d]]$  code with  $n$  physical qubits,  $k$  logical qubits, and distance  $d$ , the number of linearly independent generators is  $r = n - k$ . A stabilizer code qualifies as a QLDPC code if each qubit supports a constant number of stabilizer generators and each generator has a constant weight independent of  $n$ . A stabilizer code is classified as a CSS code [7, 31] if each generator is a tensor product of  $X$  and  $I$  or a tensor product of  $Z$  and  $I$ . Although the surface code is a QLDPC code, its encoding rate  $k/n$  approaches zero as  $n$  approaches infinity, contributing to its high overhead. In contrast, alternative QLDPC codes maintain asymptotically constant encoding rates while preserving or improving the  $d = \mathcal{O}(\sqrt{n})$  distance scaling of the surface code [16, 32–37].

Based on its stabilizer description, one can construct the Tanner graph  $T(S) = (V_q \sqcup V_S, E)$  of a QEC code. This graph includes a vertex  $q \in V_q$  for each data qubit and a vertex  $s \in V_S$  for each stabilizer generator. An edge  $(q, s) \in E$  exists between vertices  $q \in V_q$  and  $s \in V_S$  if the generator  $s$  acts non-trivially on qubit  $q$ . The Tanner graph of a QLDPC code has a degree bounded by the constant  $\mathcal{W}$ , called the sparsity of the graph.

To check whether the encoded quantum information has left the logical subspace, the stabilizer generators are measured. Assuming the  $n$  data qubits are in a code state, we expect a  $+1$  outcome for all stabilizer generator measurements. A  $-1$  outcome signals an error that anticommutes with the corresponding generator. These measurement outcomes form a classical syndrome, which is then used as input for a decoding algorithm to correct the errors while preserving the original logical state.

For CSS codes, the stabilizer generators either all involve measurements in  $X$  or  $Z$  basis. Thus, the decoding problem can be done separately for  $x$  and  $z$  errors. For example, the feasible  $z$  error configurations  $e_z$  are given by  $s_x = H_x e_z$ , where  $H_x$  is the parity check matrix for  $X$  stabilizers and  $s_x$  the syndrome outcomes. One can similarly define for  $x$  errors  $s_x = H_z e_x$ . By determining the correct  $e_z$  configuration, we can apply correction operations to correct the error. As long as the number of errors is smaller than  $\lfloor d/2 \rfloor$ , one can always find a correction operation that does not introduce a logical error. Given  $s_x = H_x e_z$ , there are multiple feasible error configurations  $e_z$ . Decoding aims to find the error that has most likely occurred, e.g. the error with the lowest weight. There are many different kinds of decoders with varying speed and accuracy, such as decoders based on maximum-likelihood [38], tensor-networks [39], minimum-weight perfect matching [40], neural-networks [41] or union-finding [42]. The popular choice for surface codes, minimum-weight perfect matching, requires that each error affects at most two stabilizer generators such that the decoding problem can be mapped onto a graph [43]. For QLDPC codes this is not possible in general. In this work, we use Belief propagation with the Ordered Statistics postprocessing step Decoder (BP-OSD) proposed in Ref. [44, 45]. Belief propagation is a heuristic message passing algorithm that estimates the single-bit marginals of a probability distribution. Here, we study depolarizing noise affecting each data qubit with error probability  $p$ , which we represent with the Kraus maps  $K_0 = \sqrt{1-p}I$  and  $K_\alpha = \sqrt{p/3}\sigma^\alpha$  with Pauli matrices  $\sigma^\alpha$ ,  $\alpha = \{x, y, z\}$  [40]. We assume that the measurement of the syndrome itself is noise-free.

## Appendix E: Outlook

To find even better low-weight codes, future research could combine our MB-QLDPC codes with subsystem codes [46, 47] and Floquet codes [48–53]. This could develop subsystem trivariate bicycle codes and Floquet trivariate bicycle codes which offer a potential avenue for a systematic approach to reducing the weight of check operators. A potential method to construct such codes is through Floquetification via ZX calculus [54, 55]. In the future, automating the discovery of MB-QLDPC with favourable parameters, such as weight, Tanner graph thickness, encoding rate, and distance, could be achieved using machine learning techniques like reinforcement learning. An interesting future work would involve analyzing the structure of polynomials analytically, allowing for the systematic discovery of MB codes with favorable parameters and Tanner Graph structure. Finally, it would be interesting to develop adaptive MB-QLDPC codes using quantum combs [56]. To further ease hardware implementation, future work studying larger QLDPC codes can also seek to optimise or provide heuristics for easing calculation of biplanarity. This could be done by leveraging on the symmetries in the Tanner Graph of QLDPC codes such as its toric layout or translation invariance, to obtain an algorithm that is not exponentially hard in system size. Specifically, the search space for possible subgraphs should be reduced to  $\text{poly}(n)$  for an algorithm to be used in a scalable search for good bi-planar QLDPC codes.

## Appendix F: Tanner Graph Details

Here, we recall the definitions used in the main text for reader convenience, but further details can be found in a standard reference such as [57]. We use the terms ‘physical’ or ‘data’ qubits to interchangeably.

Before diving into any technical details, it is important to point out that the physical implementation of a QECC does not have to directly conform to the simplest Tanner Graph structure, as long as the graph connectivity is retained. One can arbitrarily permute the qubits around physical space as they wish, changing the physical implementation of the code and the corresponding stabilizers’ supports. However, a symmetric Tanner Graph structure can greatly ease hardware implementation, by noting that the Tanner Graph embedded in  $D$ -dimensional Euclidean Space  $\mathbb{R}^D$  directly suggests one choice of physical implementation, formalized by Proposition 5. Therefore, we seek the simplest possible embedding in physical space, which in the case of MB codes is the toric layout.

Recall that the Tanner Graph of any CSS code is a bipartite graph  $(V_{\text{check}} \cup V_{\text{data}}, E)$ , such that any edge  $e$  connects some physical qubit  $v_{\text{data}}$  to some check  $v_{\text{check}}$ . Bipartite here refers to the fact that there are no connections between check vertices, and similarly no checks between physical qubit vertices. Checks and their action on physical qubits are completely specified by the Tanner Graph, thus specifying the Tanner Graph specifies a code.

Given a graph  $G$ , we now rewrite vertices of  $G$  into indices  $\{i\}$ , and the edges of  $G$  into a matrix, called the adjacency matrix  $A$ , where  $a_{ij} = 1$  when there is an edge between vertex  $i$  and vertex  $j$ , 0 otherwise. Thus, the  $A_i$  and  $B_j$  terms that make up  $A$  and  $B$  in our definition of a MB-QLDPC code, give rise to the adjacency matrix of the code’s Tanner Graph.

We formally define an embedding as a map  $E: G \rightarrow (\mathbb{R}^D)^{|V|} \times (\mathbb{R}^D)^{|E|}$ . The first argument of  $(\mathbb{R}^D)^{|V|} \times (\mathbb{R}^D)^{|E|}$  will specify the locations of the  $|V|$  vertices as distinct points, and the second argument will specify the location of the  $|E|$  edges as continuous curves.

An interaction vector  $(i, j)$  of a Tanner Graph embedding is defined as a vector that starts from data qubit vertex and ends on a check qubit vertex, the two being connected by an edge.

Define a qubit two-block CSS code as CSS codes such that  $H_X = [A|B]$  and  $H_Z = [B^T|A^T]$ , where  $A$  and  $B$  commute and have the same size. Two-blocks allow us to partition data qubits into  $L$  and  $R$  qubits. TB codes are a special type of two-block CSS code, amongst others that have been studied where  $A$  and  $B$  arise from a group algebra [58].

Proposition 5 below should be well known amongst specialists in the field, but we state it for clarity.

**Proposition 5** (Tanner Graph Physical Implementation). *Suppose  $\exists M \in \mathbb{R}$ ,  $\exists$  an embedding  $E: G \rightarrow (\mathbb{R}^D)^{|V|} \times (\mathbb{R}^D)^{|E|}$  of the Tanner graph with an upper bounded vertex density  $\rho \leq M$  (vertices per unit volume) in  $\mathbb{R}^D$ , such that  $\forall$  check vertex  $v_S$ , every data qubit sharing an edge with  $v_S$  is within distance  $r_S$ .*

*Then  $E$  provides a physical implementation of qubits of the code in  $\mathbb{R}^D$  such that the support of each stabilizer  $S$  lies in within a ball of radius  $r_S$ , determined by the embedded Tanner Graph.*

*Proof.* The point of having an upper bounded vertex density  $\rho$  is so that we don’t try to ‘game’ the system and place an increasing number of vertices per unit volume, which would allow a pathological example such as an arbitrarily large expander graph to embed into  $\mathbb{R}^D$ . In principle, we could allow for such cases but they are experimentally impractical above some density  $\rho$  due to squeezing too many qubits near one another. Essentially, we would like to focus on a physically realistic tiling of qubits on  $\mathbb{R}^D$ .

We choose the physical embedding  $E$  of qubits provided in the hypothesis, such that each stabilizer  $S$  is supported in its ball of radius  $r_S$ , specifically on those data qubit vertices that share an edge with the check vertex of  $S$ . In our paper, this refers to the toric layout embedded on a lattice in  $S^1 \times S^1$ , and indeed all for our weight-5 [30, 4, 5] code in Fig 1, our stabilizers will be supported on 4 neighbouring qubit sites, and 1 long-range qubit site.  $\square$

Note that the above proposition also implies that for any QECC such that its Tanner Graph has a local embedding in  $\mathbb{R}^D$ , the QECC parameters  $\llbracket n, k, d \rrbracket$  must satisfy the Bravyi-Poulin-Terhal bound [27], the statement that for geometrically local codes,  $\exists$  geometric locality constant  $c$  such that  $kd^{\frac{2}{D-1}} \leq cn$ . This bound holds even if one chooses a non-local physical implementation. Thus, one should remain cautious about the performance of a code, even when provided with a non-local embedding of its Tanner Graph, as it may be graph isomorphic to a geometrically local code, where the notion of a graph isomorphism is defined below in Definition 5.

**Definition 2** (Planar). *Let  $G = (V, E)$  be a graph.  $G$  is said to be planar if there exists an embedding  $E: G \rightarrow (\mathbb{R}^2)^{|V|} \times (\mathbb{R}^2)^{|E|}$  such that:*

1. *No curves intersect except at their endpoints.*

2. No point is included in more than one arc except as an endpoint.

**Definition 3** (Subgraph). A subgraph  $S = (V_S, E_S)$  of  $G = (V, E)$  is a graph such that  $V_S \subset V$  and  $E_S \subset E$ . In other words, every vertex and edge of  $S$  is a vertex and edge of  $G$  respectively.

**Definition 4** (Thickness). The thickness  $\theta$  of a graph  $G = (V, E)$  is the minimum number of planar subgraphs  $\{S_i\}_{i=1,\dots,\theta}$ , where each  $S_i = (V_i, E_i)$ , such that the edges of  $G$  can be partitioned into such that  $\cup_i V_i = V$  and  $\cup_i E_i = E$ .

**Proposition 6** (Bi-planar Architecture). All TB-QLDPC codes of weight-4, where  $A = A_1 + A_3$ ,  $B = B_1 + B_3$ , all codes of weight-5 such that  $A = A_1 + A_3$ ,  $B = B_1 + B_2 + B_3$ , and all codes of weight-6 such that  $A = A_1 + A_2 + A_3$ ,  $B = B_1 + B_2 + B_3$  (as presented in [20]), or  $A = A_1 + A_3$ ,  $B = B_1 + B_2 + B_3 + B_4$  allow for a bi-planar architecture of thickness  $\theta = 2$ , with a bi-planar decomposition attained in time  $O(n)$ .

*Proof.* For cases weight-4 and 5, we can directly carry over ‘planar-wheel’ proofs for the degree-6 graphs in Lemma 2 of [20], where in their work  $A = A_1 + A_2 + A_3$  and  $B = B_1 + B_2 + B_3$ , by setting  $A_2 = B_2 = 0$  for weight-4 codes, and setting just  $A_2 = 0$  for weight-5 codes. We will also have an identical proof structure, just with empty edges on locations where the terms are set to zero.

For cases weight-6 where  $A = A_1 + A_3$ ,  $B = B_1 + B_2 + B_3 + B_4$ , we now partition  $G$  into two subgraphs  $G_\gamma$  and  $G_\eta$  where the CSS codes representing subcodes  $\gamma$  and  $\eta$  have parity check matrices as follows:

$$H_\gamma^X = [A_1 | B_1 + B_2] \quad \text{and} \quad H_\gamma^Z = [B_1^T + B_2^T | A_1^T] \quad , \quad H_\eta^X = [A_3 | B_3 + B_4] \quad \text{and} \quad H_\eta^Z = [B_3^T + B_4^T | A_3^T] \quad (\text{F1})$$

This allows a bi-partition into two degree-3 subgraphs, allowing us to adapt the proof of [20] on each degree-3 subgraph of our weight-6 codes.  $\square$

Note that the above proof breaks down if we have  $A = A_1 + A_3$ ,  $B = B_1 + B_2 + B_3 + B_4 + B_5$  such as in our weight-7 code. It is easy to extend the above argument to show that weight-7,8,9 codes have a thickness-3 implementation (and analogously for larger weights and thickness), by splitting into 3 CSS subcodes, but high thickness is not desirable for near-term hardware implementation. The Tanner Graph is degree-7, but it is known that degree-7 thickness-2 graphs exist, such as the complete  $K_7$  graph, defined as having 7 vertices and all-to-all connectivity [57]. Furthermore, a lower bound on graph thickness is obtained from a corollary of Euler’s polyhedron formula, that given a graph with  $p$  vertices and  $q$  edges,  $\theta \geq \frac{q}{3p-6}$  [59], yielding a lower bound of  $\theta \geq \frac{25}{29}$  for our weight-7 [30, 4, 5] codes. It is easy to verify that the graph is not planar, but we could remain hopeful that it has thickness  $\theta = 2$ .

In order to rule out the possibility that the graph may fortunately be of thickness  $\theta = 2$ , a numerical program is necessary. Furthermore, by explicitly checking subgraphs, we will obtain an bi-planar layout for experimental realization. This brute-force procedure for checking  $\theta=2$  is generically NP-complete [60]. For very small codes such as the Shor Code [6], it is still practical to enumerate decompositions into 2 subgraphs, and then check the planarity of each subgraph. However, our weight-7 [30, 4, 5] code did not provide an answer after a few days of simulation. An upper bound provided below on the computational complexity of a brute-force search for bi-planarity suggests that the difficulty of iterating over subgraphs is the key area for improvement in aiming towards a  $\text{poly}(n)$  time complexity.

**Proposition 7** (weight- $\mathcal{W}$  QLDPC Graph Bi-planarity Test Complexity). For any QLDPC code of sparsity  $\mathcal{W}$ , recall that its Tanner Graph will have degree  $\mathcal{W}$ . Then testing for bi-planarity is  $\mathcal{O}(n 2^n)$ .

*Proof.* We analyse the main steps in testing of bi-planarity:

1. Breaking the Tanner Graph into 2 subgraphs allows for  $\sum_{i=1,\dots,n} \binom{n}{i} = 2^n$  choices of subgraphs.
2. Looping over each subgraph choice, we test for planarity using the Left-Right Planarity Test with  $\mathcal{O}(e)$  complexity [61], where  $e$  is the number of edges of the graph being tested for planarity. In the Tanner Graph with sparsity  $\mathcal{W}$ , we have  $e = \mathcal{O}(\mathcal{W}n)$ , thus the planarity test for both subgraphs is  $\mathcal{O}(n)$ .

Putting them together, we get an upper bound of  $\mathcal{O}(n 2^n)$ , an exponential time complexity.  $\square$

At this point, it is worth noting that we could generically define a  $b$ -block group algebra code as  $[A_1 | A_2 | \dots | A_b]$ , enforce that  $\sum_i A_i A_{k-i+1}^T = 0$  to enforce the CSS condition, and study it as a qLDPC code. We expect the generic framework to carry over.

**Definition 5** (Graph Isomorphism). *Two graphs  $G$  and  $H$  are isomorphic if there exists a bijection*

$$g : V(G) \rightarrow V(H)$$

*from the vertices of  $G$  to the vertices of  $H$ —such that any two vertices  $u$  and  $v$  of  $G$  have an edge in  $G \iff g(u)$  and  $g(v)$  have an edge in  $H$ .*

*Intuitively, we can relabel the vertices and edges of  $G$  to get those of  $H$ . This is what allows us to view the Tanner Graph of MB-QLDPC codes on the discrete torus.*

Physical qubits are now bipartitioned into L and R qubits,  $\frac{n}{2} = lm$  qubits each. L and R refer to the left and right blocks in the check matrix definition,  $H_X = [A|B]$  and  $H_Z = [B^T|A^T]$ .

A Cayley Graph is essentially the ‘natural graph structure’ endowed onto any group, defined through the generators of a group. We focus on undirected Cayley Graphs, which have undirected edges.

As in Ref [20], we re-define physical qubits and checks as each labelled by monomials,  $M = \{x^i y^j \mid i = 0, 1, \dots, l-1, j = 0, 1, \dots, m-1\}$ . We view the monomials  $M$  as a multiplicative group isomorphic (by a map  $f^{-1}$  below) to the additive group of  $\mathbb{Z}_{lm} = \{0, 1, \dots, lm-1\}$ . Visually, we can represent both objects ( $M$  and  $\mathbb{Z}_{lm}$ ) by a planar x-y grid of  $l \times m$  points. These points on the grid are not qubits, but rather a collection of 4 objects, which consists of an L qubit, an R qubit, an X-check, a Z-check. Thus, this notation assigns each qubit or check a label  $q(T, \alpha)$ , where  $T \in \{L, R, X, Z\}$  is the data type and  $\alpha \in M$  is the monomial label.

$$f : (+, \mathbb{Z}_{lm}) \rightarrow (\times, M), f(i) = x^{a_i} y^{i-ma_i} \quad \text{where} \quad a_i := \lfloor \frac{i}{m} \rfloor$$

This isomorphism basically indexes along the x-axis from 0 to  $l-1$  and along the y-axis from 0 to  $m-1$ . Multiplying by x corresponds to addition by m in  $\mathbb{Z}_{lm}$ , moving points along the x-y grid horizontally by a unit. Multiplying by y corresponds to addition by 1 in  $\mathbb{Z}_{lm}$ , moving points along the x-y grid vertically by a unit. Since our third variable  $z = S_l \otimes S_m = xy$  is contained in  $M$ , we have left  $M$  unchanged under the introduction of variable  $z$ , allowing us to modify Lemma 3 and 4 of Ref [20] to study the Tanner Graph of our codes.

In this framework,  $\forall$  points  $\alpha \in M$ ,  $q(L, \alpha)$  data qubits have the set of X-check neighbours  $L_X = \{A_i^T \alpha \mid i = 1, \dots, \mathcal{W}_A\}$  an Z-check neighbours  $L_Z = \{B_i^T \alpha \mid i = 1, \dots, \mathcal{W}_B\}$ . Similarly,  $q(R, \alpha)$  data qubits have the set of X-check neighbours  $R_X = \{B_i^T \alpha \mid i = 1, \dots, \mathcal{W}_B\}$  and Z-check neighbours  $R_Z = \{A_i \alpha \mid i = 1, \dots, \mathcal{W}_A\}$ .

**Definition 6** (Cayley Graph). *Given a group  $C = \langle c \rangle$  with generators  $c$ , the Cayley Graph  $\Gamma(C, \{c\})$  is defined as the graph such that*

1. *Vertices are the elements of  $c \in C$*
2.  *$\forall g \in C$ ,  $\forall$  generator  $c$ , there is an undirected edge between  $g$  and  $gc$ .*

*For  $\mathbb{Z}_a \times \mathbb{Z}_b$ , its Cayley graph is the Cayley Graph generated by  $\{(1, 0), (0, 1)\}$ . Its Cayley Graph can geometrically be interpreted as a discrete torus with non-contractible cycles of length  $a$  and  $b$ , vertices being the vertex of the torus, edges being the grid lines of the torus.  $(1, 0)$  and  $(0, 1)$  would represent a unit shift along the x-direction and the y-direction respectively.*

**Definition 7** (Spanning Subgraph). *A spanning subgraph  $S$  of a graph  $G$  is a subgraph that contains all the vertices of  $G$ , but not necessarily all the edges.*

The next point to address is showing translational symmetry of edges on this toric layout that emerge from the X and Z check vertices. Once we establish translational symmetry, we can find the long-range edges by first noting that the toric layout provides a re-indexing map of the vertices into tuples on the square grid,  $f : V \rightarrow \{(i, j) \mid i = 1, \dots, 2\mu \text{ and } j = 1, \dots, 2\lambda\}$ . Given a vertex at position  $(i, j)$ , after identifying the position  $(i', j')$  of the long-range edge’s adjacent vertex, we obtain the interaction vectors  $(i' - i, j' - j)$ . Note that X and Z checks can have different interaction vectors.

Recall the formal definition of an embedding  $E : G \rightarrow (\mathbb{R}^D)^{|V|} \times (\mathbb{R}^D)^{|E|}$ . In the proposition below, we say that a graph  $G$  is overlapped onto another graph  $H$  when embeddings  $E_G$  and  $E_H$  are chosen such that  $E_G(G) = E_H(H)$  in  $(\mathbb{R}^D)^{|V|} \times (\mathbb{R}^D)^{|E|}$ . Note that two graphs  $G, H$  can be overlapped  $\iff G, H$  are graph isomorphic.

**Proposition 8** (TB-QLDPC Toric Layout Criterion for arbitrary weight, generalised from Ref. [20]). *A TB-QLDPC code  $(QC(A, B))$  of weight  $\mathcal{W} = \mathcal{W}_A + \mathcal{W}_B$  has a toric layout  $\iff \exists i, j \in \{1, \dots, \mathcal{W}_A\}, g, h \in \{1, \dots, \mathcal{W}_B\}$  such that*

1.  $\langle A_i A_j^T, B_g B_h^T \rangle = M$  and
2.  $\text{ord}(A_i A_j^T) \text{ord}(B_g B_h^T) = lm$ .

To explain the idea behind Proposition 8, which gives our criterion for a toric layout, split our data qubits into two blocks through the definition below.

$$H_X = [A|B] \quad \text{and} \quad H_Z = [B^T|A^T]$$

L represents first half of the qubits (left side of block matrix), R represents the second half (right side of block matrix).

Our goal is to place the vertices of our Tanner Graph on the discrete torus indexed by  $\mathbb{Z}_{2\mu} \times \mathbb{Z}_{2\lambda}$ , but we allow for edge crossings. The intuition is that we need to look for a uniform choice of edge label to traverse between X checks (say X and X') in a cyclic manner, similarly for Z checks. Thus we have to choose an  $A_j^T$  to go from X to L, and  $A_i$  for L to X', similarly a  $B_h^T$  and  $B_g$  for R physical qubits and Z checks. Therefore,  $A_i A_j^T, B_g B_h^T$  are the various monomials generated by our individual terms in the A and B matrices, representing 2-step crossings between X checks and Z checks respectively on the Tanner Graph. We fix a given X check vertex as 1, the identity, and multiply by  $A_i A_j^T$  until we get back to 1. Therefore,  $\text{ord}(A_i A_j^T) = \mu$ , where the order of the element determines how many 2-steps are made in a direction, starting from an X check before we return to the same X check. A similar argument follows for  $\text{ord}(B_g B_h^T) = \lambda$  and Z checks. Thus, the Tanner Graph can be viewed on the torus  $\mathbb{Z}_{2\mu} \times \mathbb{Z}_{2\lambda}$ .

**Proposition 9** (TB-QLDPC Toric Layout Edge Translational Invariance). *For any TB-QLDPC code (with Tanner Graph G) of sparsity  $\mathcal{W}$  with a toric layout, for any vertex  $v_T$  of a fixed type  $T \in \{L, R, X, Z\}$ , all of the  $\mathcal{W}$  edges of  $v_T$ , including the long-range edges, have translationally invariant interaction vectors on the toric layout.*

*Proof.* We first define two concepts relevant in our TB codes.

Circulant matrices  $C$  are matrices such that if  $(c_0, c_1, \dots, c_r)$  is row-r of the matrix, then  $(c_i, c_0, c_1, \dots, c_{i-1})$  is row- $(r+1)$  of the matrix, the rows are shifted right by one position. Because a circulant matrix  $C$  can be diagonalized into  $C = FDF^{-1}$  using a Discrete Fourier Transform  $F$ , where  $\omega = e^{\frac{2\pi i}{N}}$  and the action of  $F$  is defined as  $F |j\rangle = \sum_{k=1}^{N-1} \omega^{-jk} |k\rangle$ , we conclude that its  $k$ -th power  $C^k = F^{-1} D^k F$  is also a circulant matrix.

Cyclic matrices are matrices such that if  $\exists (c_0, c_1, \dots, c_r)$  is a row of the matrix, then  $(c_i, c_0, c_1, \dots, c_{i-1})$  is also a row of the matrix. Note that if A and B are circulant, then  $A \otimes B$  is cyclic.

We use the isomorphism provided above, recalled here for convenience.

$$f : (+, \mathbb{Z}_{lm}) \rightarrow (\times, M), f(i) = x^{a_i} y^{i-ma_i} \quad \text{where} \quad a_i := \left\lfloor \frac{i}{m} \right\rfloor$$

On the 2-D x-y grid defined by the isomorphism  $f$ , as mentioned we view L and R data qubits, X and Z checks to tile the grid,  $4lm$  vertices in total, with one combined  $(L, R, X, Z)$  unit per point. We do not define edges between data qubits and check vertices yet.

Recall that the TB codes are defined using shift matrices  $x, y, z = S_l \otimes I_m, I_l \otimes S_m, S_l \otimes S_m$ .  $S_l$  and  $S_m$  are circulant matrices. Thus  $x, y, z$  are cyclic matrices.

Furthermore,  $A_i$  being a power of some variable  $x, y, z$ , is a tensor product of circulant matrices, thus cyclic. Since  $A_i$  is cyclic, for a fixed row  $r$ , it has non-vanishing entries on a set  $\{(a_{i_1}, \dots, a_{i_{W_A}})\}$ , which is translationally-invariant on the x-y grid because  $A_i$  is cyclic, thus  $\exists r'$  such that  $\{(a_{i_{W_A}}, a_{i_1}, \dots, a_{i_{W_A-1}})\}$ .

For each  $A_i$  term introduced, we have for each vertex  $v$  an edge  $e_{v,X}$  along the grid to some X-check, call it X. Similarly we have  $e_{v,Z}$  to a Z-check called Z. Due to the  $A_i$  being cyclic, the edges introduced are translationally invariant (with PBC) on the x-y grid defined by the isomorphism  $f$ . Note that at this point, we have not imposed any requirement of a toric layout structure.

We may add as many edges as we like by introducing more terms  $A_i$  and  $B_j$ , and they remain translationally invariant by repeating the argument above.

Furthermore, now using our hypothesis that the code has a toric layout, we may now traverse along the edges that define the toric grid, as per Proposition 2 to make them overlap on the Cayley Graph of  $\mathbb{Z}_{2\mu} \times \mathbb{Z}_{2\lambda}$  embedded in  $\mathbb{R}^2$  with PBC. Since the graph is translationally symmetric, all the edges have translationally symmetric interaction vectors, including the long-range edges.  $\square$

Such translation invariant codes generated by cyclic matrices have also been studied in the literature, such as bicycle codes and two-block quantum group algebra codes [21, 58].

**Definition 8** (Twisted Toric Layout). A CSS QLDPC code  $C$  has a  $(t_x, t_y)$ -twisted toric layout  $\iff \exists$  positive integers  $t_x, t_y$  such that the Tanner Graph of  $C$  has a toric layout, upon imposing an additional shift of  $t_x$  units along the  $x$ -direction of the periodic boundary conditions of the toric layout, similarly for  $t_y$  along the  $y$ -direction.

Note the above definition has a positive or negative direction ambiguity. We fix it to be shifts along the positive direction.

By this definition, the codes with a toric layout such as in Fig 1 will have  $t_x = t_y = 0$ , the trivial twist. Non-trivial twisted toric layouts no longer have global translational symmetry, but retain it in the bulk. Some work has been done on studying twisted layouts [62], and it can be fruitful to find a systematic way to incorporate such theoretical results in a search for desirable weight-4 QLDPC codes for near-term implementation, as a first step beyond the toric code.

**Definition 9** (Tangled Toric Layout). A CSS QLDPC code  $C$  has a  $(\sigma, \tau)$ -tangled toric layout  $\iff \exists \sigma \in S_{2\mu}, \tau \in S_{2\lambda}$  where  $S_q$  is the permutation group on  $q$  elements, such that the Tanner Graph of  $C$  has a toric layout after applying  $\sigma$  along the  $x$ -direction of the periodic boundary conditions of the toric layout, similarly for  $\tau$  along the  $y$ -direction.

The notion of tangled toric layout can be considered the most general case for disrupting the PBC of the torus, whilst keeping the horizontal and vertical PBC's separate. Note that the twisted layout definition is a special case of a tangled layout, corresponding to  $\sigma$  being the permutation cycle that sends  $i$  to  $i + t_x \bmod 2\mu \forall i$ , and similarly  $\tau$  sends  $j$  to  $j + t_y \bmod 2\lambda \forall j$ .

We encourage readers to find systematic ways of studying tangling parameters  $(\sigma, \tau)$  of codes that are surface codes in the bulk. As a first step in this direction, we provide one algorithm below for weight-4 TB codes that have a tangled toric layout.

**Proposition 10** (Algorithm for Weight-4  $(\sigma, \tau)$ -Tangled Toric Layout Parameters). For any two-block CSS QLDPC code of sparsity 4 with equal  $X$  and  $Z$  degree per data qubit (2 each), suppose it has a tangled toric layout known to have torus parameters  $\mu, \lambda$ .

Then there is an  $O(n)$  time algorithm to find  $\sigma, \tau$ .

*Proof.* It is instructive to refer to Fig 1 while reading this proposition, ignoring the long-range edges. The key idea is to embed a spanning subgraph onto the rectangular grid of size  $2\mu \times 2\lambda$ . The remaining edges on the boundary left unassigned to the square grid along x-direction and y-direction give us  $\sigma$  and  $\tau$  respectively. We analyse the main steps:

1. A choice for the top-right vertex of the 2-D grid is made, it can be arbitrary. Fixing it as a data qubit, 2 distinct X and Z vertices are chosen to the left and below it. The other 2 are left unassigned, they are part of the boundary.
2. Recall that by hypothesis, the CSS Tanner Graph is bipartite (into data qubits and checks) and degree-4. Our challenge now is to decide which data qubit type, L or R, should be placed along the horizontal axis of the embedding. A poor choice such as placing two L qubits diagonally adjacent to each other on the square grid, would prevent us from getting a layout like Fig 1. This is where the L-R split of data qubits is crucial. Recall that we can bipartition L and R by using the left and right blocks in the check matrix definition,  $H_X = [A|B]$  and  $H_Z = [B^T|A^T]$ . The first half of the data qubit indices are in L, and the second half indices are in R. Thus, at an X check  $v_X$ , we choose the data qubit to its left to be an L qubit  $v_L$ , and the data qubit below it to be an R qubit,  $v_R$ . Finally, we place any Z-check ( $v_Z$ ) that shares an edge with  $v_R$  to the right of  $v_R$ . This allows us to produce a  $2 \times 2$  unit cell of the Tanner Graph embedding, consisting of 1 of each vertex type (X, Z, L, R).
3. We repeat the above assignment rules for each vertex by continuing to assign directions of data qubits and checks on the square grid based off the L-R split. As a result, the arrangement of all other vertices on the grid are uniquely specified (refer to Fig 1), by ‘snaking’ our way from right to left, then moving to the next row, assigning vertices from the left to right, iteratively tessellating unit cells all the way down the 2-D grid. This step is  $O(n)$  time complexity.
4. By ignoring the bulk of the grid and only looking at the top and bottom edges of the 2-D grid defined along the x-direction boundary, we obtain a bipartite graph with two rows of vertices, and edges only between the rows, but not within each row. This bipartite graph is just a visual representation of a bijective map. This bijection defines a permutation map  $\sigma$  for us upon indexing the qubits along the boundary by integers. There is no loop in this step of the algorithm, thus this step is additive in time complexity. This step is  $O(\sqrt{n})$  because we only enumerate the along the perimeter of the 2-D grid, which has  $O(\sqrt{n})$  vertices.

5. We repeat Step 4 along the y-direction for the left and right vertical edges, to obtain  $\tau$ .

□

The above algorithm also works for even more general notions of tangling, where the x and y boundary conditions may mix. In such cases,  $(\sigma, \tau)$  parameters will be combined into a single tangling parameter  $\gamma \in \text{Bij}(V_x \cup V_y)$ ,  $\gamma$  being a permutation of the combined boundary vertices.  $V_x$  is the vertices along the x-direction, similarly for  $V_y$ .

The above proposition holds higher-weight codes, assuming additionally that one knows beforehand the choice of a spanning subgraph for a toric layout. However, this choice is generally not clear a priori. One would have to iterate through various choices of edges in the spanning subgraph, which is exponentially hard. For weight-4 codes, it suffices to know what  $\mu, \lambda$  are, since the Tanner Graph is degree-4, leaving no freedom in the choice of edges on the spanning subgraph. Furthermore, it is easy to deduce  $\mu, \lambda$  by using computer vision tools or visual inspection of the Tanner Graph, such as in Fig 4.

One possible direction for further optimization of ultra low-weight codes is to explore the questions: What are the ideal forms of tangling for improving code parameters, decoding and hardware implementation? Concretely, this can be done by imposing further structure on tangling parameters  $(\sigma, \tau)$  in a torus to improve code performance, of which a  $(t_x, t_y)$  twisted toric layout is only one of many possibilities [62]. We expect improved performance by a constant factor, but not in the asymptotic scaling.